Journal of Materials Chemistry B

ROYAL SOCIETY OF CHEMISTRY

PAPER

View Article Online
View Journal

Cite this: DOI: 10.1039/d6tb00055j

Fabrication of near-infrared-light-responsive photothermal tea leaf-derived particles with thermotolerance inhibitory and anticancer activities

Keito Suzuki,[a] Syuuhei Komatsu,[a] Kanae Ishii,[a] Kaho Tanaka,[a] Yuka Kiba,[a] Masashi Kitamua,[a] Toru Kimura,[a] Ryuichiro Suzuki,[a] Takashi Tanikawa,[a] Kazuya Oki,[b] Atsushi Takahashi[b] and Hiroaki Todo*[a]

Photothermal therapy (PTT) combined with chemotherapy is a promising cancer treatment approach, but its effectiveness is limited due to concerns about heat resistance mediated by heat shock proteins (HSPs) and the side effects of chemotherapy. In this study, we developed indocyanine green (ICG)-encapsulated tea leaf nanoparticles (TLNPs-ICG) as a photothermal nanoplatform. The TLNPs, approximately 140 nm in diameter, efficiently encapsulated ICG and demonstrated stable, concentration-dependent photothermal heating under 800 nm near-infrared irradiation. TLNPs-ICG were readily internalized by keratinocytes and melanoma cells, likely *via* the EGCG/67 kDa laminin receptor, and exhibited selective cytotoxicity against melanoma cells. When combined with near-infrared irradiation, TLNPs-ICG exhibited potent photothermal cell killing, whereas TLNPs or free ICG alone was only marginally effective. Importantly, TLNPs-ICG attenuated the upregulation of HSP70 and HSP90 and suppressed the acquisition of thermotolerance *in vitro* and *in vivo*. In a B16 melanoma mouse model, the intratumoral administration of TLNPs-ICG, combined with intermittent near-infrared irradiation, significantly suppressed tumor growth without apparent systemic toxicity. These results suggest that TLNPs-ICG are plant-derived biomaterials that integrate EGCG-mediated biochemical activity, heat shock regulation, and ICG-mediated photothermal effects, providing a platform for next-generation PTT-combined cancer therapy.

Received 7th January 2026,
Accepted 16th March 2026

DOI: 10.1039/d6tb00055j

rsc.li/materials-b

Introduction

Hyperthermia is a well-established cancer treatment method that uses external stimuli, such as light or an alternating magnetic field, to locally heat tumor tissues to approximately 43 °C.[1,2] Under well-controlled conditions, hyperthermia can be applied minimally invasively and can preferentially damage malignant cells while sparing surrounding normal tissue. It can be combined with surgery, radiation therapy, and chemotherapy to enhance therapeutic efficacy. Photothermal therapy (PTT) is a representative form of hyperthermia. It involves administering a photothermal agent into the body and converting the absorbed energy into heat by irradiating the tumor with light, thereby increasing the tumor temperature and killing cancer cells.[3,4] Near-infrared (NIR) light is particularly widely used for PTT due to its relatively high tissue penetration and low inherent phototoxicity. Combination strategies that integrate PTT with conventional chemotherapeutic agents are attractive because heat enhances the pharmacological activities of anticancer drugs, enabling more efficient treatment.[5,6] However, such approaches also raise concerns about off-target toxicity to normal tissues. Furthermore, heat exposure induces the production of heat shock proteins (HSPs), such as HSP70 and HSP90, promoting thermotolerance in tumor cells.[7] As a result, the effectiveness of repeated PTT sessions tends to decrease over time as tumors adapt to heat stress. Therefore, to maximize the effectiveness of PTT, a photothermal therapy agent that not only generates heat under near-infrared irradiation but also suppresses HSP induction and preferentially targets cancer cells is highly desirable.

Epigallocatechin-3-gallate (EGCG), a major polyphenolic catechin abundant in green tea leaves, has attracted attention in cancer treatment.[8–10] EGCG binds to the 67 kDa laminin receptor (67LR), which is overexpressed on the surface of many cancer cells, and exerts its anticancer effects through this interaction.[11,12] Furthermore, EGCG has been reported to inhibit the expression of HSP70 and HSP90, which are important molecular chaperones involved in the development of

[a] Faculty of Pharmacy and Pharmaceutical Sciences, Josai University, 1-1 Keyakidai, Sakado, Saitama 350-0295, Japan. E-mail: ht-todo@josai.ac.jp; Fax: +81-49-271-8137; Tel: +81-49-271-7943
[b] Saitama Tea Research Institute, 244-2 Kamiyaganuki, Iruma-shi, Saitama, Japan

thermotolerance.[13,14] These properties suggest that EGCG may be a promising adjuvant for PTT by conferring tumor selectivity while attenuating the heat shock response. However, EGCG suffers from poor stability. EGCG is prone to degradation and structural changes in response to environmental factors, such as light, pH, ionic strength, and temperature. To improve its stability and bioavailability, various strategies have been explored, including co-formulation with ascorbic acid,[15] complexation with proteins or other carrier molecules,[16,17] and encapsulation within liposomes or related nanocarriers.[18,19] While these approaches can enhance EGCG stability, they often require laborious carrier preparation processes, potentially increasing formulation complexity.

Plant-derived nanoparticles (pdNPs) have recently emerged as a new class of bioinspired nanocarriers with potential advantages for drug delivery and disease treatment.[20–22] pdNPs are exosome-like nanoparticles isolated and purified from plant sources. They consist of heterogeneous vesicles, membrane fragments, and organelle-like structures. Nanoparticles isolated from plants, such as ginseng,[23] ginger,[24] grapefruit,[25] and grapes,[26] have been reported to encapsulate plant-derived bioactive molecules, proteins, and nucleic acids and are being investigated as carriers for targeted delivery and therapeutic intervention. Because pdNPs are primarily composed of various phospholipids and other membrane components, they are expected to enable functional modifications similar to those of conventional liposomes while maintaining the biocompatibility and bioactivity associated with their plant origin. Some of these particles have also been reported to exhibit anticancer activities, making them useful as therapeutic materials.[23,24] Recently, the design of aloe-derived nanoparticles containing indocyanine green for hyperthermia, which generate heat in response to near-infrared light, has been reported. However, considerations remain to be made regarding the development of thermotolerance through the production of HSPs.[27] Most ICG delivery systems reported to date include synthetic liposomes, polymeric nanoparticles, and plant-derived nanoparticles (*e.g.*, ginger, grapefruit, and aloe-derived pdNPs), primarily designed to improve ICG stability and tumor accumulation. However, photothermal therapy using these particles still faces a significant biological barrier: repeated heating, or even mild heating, can activate the heat shock response, leading to the increased expression of HSP70/HSP90 and subsequent increased thermotolerance. In many cases, these carriers function primarily as delivery vehicles and do not inherently suppress heat-induced HSP signaling. As a result, additional exogenous HSP inhibitors or concomitant medications are often required, increasing formulation complexity and potentially raising safety concerns. Tea leaf-derived nanoparticles (TLNPs), a subtype of pdNPs derived from tea leaves, stably contain tea leaf components, such as EGCG, and have been shown to exhibit antitumor activities against human and mouse breast cancer cell lines.[28] These findings raise the possibility that TLNPs may function as natural EGCG-containing nanoplatforms that exert tumor-selective and HSP-modulating effects. Currently, there are few reports on the functionalization of pdNPs, including TLNPs, for photothermal therapy, and pdNP-based materials that can essentially suppress HSP expression to achieve more effective treatment are still lacking.

Based on these considerations, we hypothesized that loading photothermal agents into TLNPs would result in multifunctional nanomaterials that could selectively target cancer cells, exert their inherent anticancer activity *via* EGCG, and simultaneously enhance the efficacy of PTT. Furthermore, the incorporation of EGCG into TLNPs can be easily performed and may suppress the expression of HSP70 and HSP90 in the tumor microenvironment, potentially preventing or mitigating the development of thermotolerance during repeated PTT cycles. However, although such a multifunctional profile is highly desirable for achieving robust antitumor efficacy, only a limited number of materials have been reported that simultaneously possess these properties. In this study, we encapsulate ICG, a clinically used near-infrared-absorbing dye with well-characterized photothermal properties, into TLNPs to create near-infrared-responsive photothermal TLNPs (TLNPs-ICG) (Fig. 1). In this study, TLNPs-ICG are developed as a multifunctional green tea-derived nanoplatform that synergistically integrates NIR-triggered photothermal heating with EGCG-mediated antitumor activity and cancer cell selectivity, while concurrently attenuating HSP70/90-associated thermotolerance, thereby enabling more effective PTT-based cancer therapy.

Experimental section

Materials

Human immortalized keratinocytes (HaCaT) were obtained from Cell Lines Service GmbH (Land Baden-Württemberg, Germany). The human malignant melanoma cell line, A375, was purchased from the European Collection of Authenticated Cell Cultures (ECACC, Porton Down, England). The murine cutaneous melanoma cell line, B16, was supplied by the JCRB Cell Bank, National Institutes of Biomedical Innovation, Health and Nutrition (Osaka, Japan). Phosphatidylinositol PI (17 : 0/20 : 4) was sourced from Avanti Polar Lipids (Birmingham, England). Indocyanine green, Dulbecco's modified Eagle's medium (DMEM), Eagle's minimum essential medium (EMEM), trypsin–EDTA, and Dulbecco's phosphate-buffered saline without calcium and magnesium [D-PBS(−)] were purchased from FUJIFILM Wako Pure Chemical Corporation (Osaka, Japan). Fetal bovine serum (FBS) was obtained from Sigma-Aldrich (St. Louis, MO, USA). The lipophilic fluorescent tracers, DiI [DiIC18(3)] and DiO [DiOC18(3)], were purchased from Setareh Biotech (Eugene, OR, USA). LysoTracker™ Green DND-26 was obtained from Thermo Fisher Scientific (Waltham, MA, USA). Rabbit polyclonal anti-HSP70 (human reactive) was purchased from Funakoshi Co. (Tokyo, Japan), and rabbit polyclonal anti-HSP90 (human reactive) was obtained from COSMO BIO Co. (Tokyo, Japan). Seven-week-old male C57BL/6 mice (body weight 17–21 g; Sankyo Labo Service Co., Ltd, Tokyo, Japan) were maintained under specific pathogen-free (SPF) conditions at Josai University. Tea leaves (*Camellia sinensis*, cultivar Kōro, harvested in October)

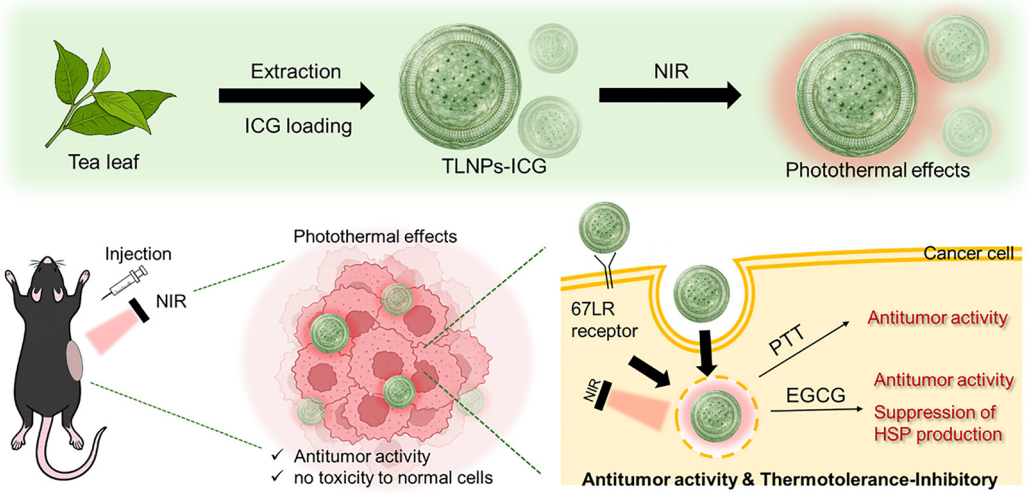

Fig. 1 Schematic of the preparation of TLNPs-ICG.

were kindly provided by the Saitama Tea Research Institute (Saitama, Japan).

Preparation of tea leaf-derived nanoparticles loaded with indocyanine green (TLNPs-ICG)

Tea leaf-derived nanoparticles (TLNPs) were isolated and purified using a reported modified sucrose cushion method.[29,30] Briefly, fresh tea leaves were homogenized in D-PBS(−) using a blender to obtain a juice-like mixture. The homogenate was then centrifuged at 3000 × *g* for 10 min at 4 °C, followed by successive centrifugations at 10 000 × *g* and 16 500 × *g* for 60 min each. After removing insoluble debris, the supernatant was passed through a 0.45 μm filter (Minisart NML, Sartorius, Göttingen, Germany) to further remove residual particles. The filtrate was carefully layered onto a 30% (w/v) sucrose cushion prepared in D-PBS(−) and ultracentrifuged at 141 000 × *g* for 90 min. The sucrose fraction containing TLNPs was collected, resuspended in D-PBS(−), and ultracentrifuged at 141 000 × *g* for 90 minutes. The resulting precipitate was collected and resuspended in 500 μL of D-PBS(−). This final suspension was designated as TLNPs. For physicochemical characterization, the TLNP suspension was diluted 10-fold with D-PBS(−), and the hydrodynamic diameter and zeta potential were measured using a Zetasizer Nano (Malvern, UK). The protein content of the recovered TLNPs was quantified by a micro bicinchoninic acid (microBCA) assay using a BCA protein assay kit. The TLNP suspension was diluted 20, 40, 60, and 80 times, and a serial dilution series for the standard curve was prepared using bovine serum albumin (BSA). Each diluted sample or BSA standard solution (25 μL) was mixed with 100 μL of a prepared working reagent in a 96-well plate and incubated at 60 °C for 30 minutes. The absorbance at 562 nm was then recorded using a microplate reader (Synergy H1, Agilent BioTek, Tokyo, Japan), and the protein concentration of the recovered TLNPs was calculated from the BSA standard curve.

ICG solution (1.0 mg mL^{-1}) and TLNP dispersion (1.0 mg mL^{-1}) were mixed at a 1 : 1 volume ratio and incubated at 37 °C for 1 hour. The suspension was centrifuged for 20 minutes, the supernatant was removed, and the resulting pellet was resuspended in D-PBS(−) to obtain ICG-encapsulated TLNPs (TLNPs-ICG). The ICG concentration in the removed supernatant was quantified, and the ICG loading amount and loading efficiency of the TLNPs-ICG were calculated. The resulting TLNPs-ICG were diluted 10-fold with D-PBS(−), and the hydrodynamic diameter and zeta potential were measured by dynamic light scattering (DLS). The amount of ICG leakage from the TLNPs-ICG was evaluated by incubating the dispersion at 37 °C for 1, 3, 6, and 24 hours, followed by centrifugation. The supernatant was collected, and the absorbance at 785 nm was measured using a microplate reader. The amount of ICG leakage was expressed as the ratio of the amount of ICG detected in the supernatant to the amount of ICG initially encapsulated in TLNPs-ICG. EGCG was quantified as indicated in a previous study,[27] with minor modifications. TLNPs were dissolved in methanol and centrifuged at 12 000 × *g* for 10 min, after which the supernatant was collected for analysis. The EGCG content in the supernatant was determined by high-performance liquid chromatography (HPLC; Shimadzu Corporation, Kyoto, Japan). Chromatographic separation was performed using solvent A (0.2% phosphoric acid in H_2O) and solvent B (methanol) as the mobile phases at a flow rate of 0.85 mL min^{-1}, with UV detection at 280 nm. The column oven was maintained at 45 °C, and an Inertsil® ODS-3 column (3.5 μm, 4.6 × 150 mm) was employed for the analysis.

Evaluation of the NIR-responsive photothermal effect of TLNPs-ICG

TLNPs and TLNPs-ICG (10, 50, and 100 μg mL^{-1}) dispersions were irradiated with near-infrared (NIR) light at 800 nm (1 W cm^{-2}) using a NIR light source (an irradiation device supplied by Iwasaki Electric Co., Ltd, Saitama, Japan). During irradiation, the temperature was recorded at 30 second intervals using thermometry and infrared thermography (Compact Thermal Camera AD-5637, A&D Co., Ltd, Tokyo, Japan) to

evaluate the photothermal response. To examine the durability of the photothermal effect, a TLNPs-ICG dispersion (50 μg mL^{-1}) was irradiated with NIR light for 8 minutes, followed by a 12 minute cooling period, which was repeated five times. The temperature was measured every 30 seconds. The cooling temperature was also recorded at 30 s intervals, and the photothermal conversion efficiency was calculated (SI).

Preparation of fluorescent-labeled TLNPs-ICG

The fluorescent labeling of TLNPs-ICG was performed as in our previous study.[28,29] TLNPs-ICG (50 μL, total protein concentration 1.0 mg mL^{-1}) were mixed with DiO and DiI (2 μL each, 500 μmol L^{-1}) and vortexed at 35 °C for 10 minutes in the dark. The mixture was then centrifuged at 122 000 × *g* for 20 minutes to obtain TLNPs-ICG with a fluorescently labeled lipid membrane.

Evaluation of the cellular uptake and cytotoxicity of TLNPs-ICG

HaCaT cells were cultured in D-MEM supplemented with 10% heat-inactivated FBS at 37 °C in a humidified atmosphere of 5% CO_2. A375 human melanoma cells were maintained under the same conditions in D-MEM supplemented with 15% heat-inactivated FBS. B16 melanoma cells were cultured in E-MEM supplemented with 10% heat-inactivated FBS at 37 °C in a humidified atmosphere of 5% CO_2. The cellular uptake of TLNPs was assessed by flow cytometry (FACS) and confocal laser scanning microscopy (CLSM). For FACS, the HaCaT, A375, and B16 melanoma cells were seeded at 1×10^5 cells mL^{-1} in 24-well plates (VIOLAMO, AS ONE, Osaka, Japan) and allowed to adhere overnight at 37 °C in a 5% CO_2 atmosphere. The culture medium was replaced with serum-free medium, and DiO-labeled TLNPs or TLNPs-ICG were added to a final concentration of 50 μg mL^{-1}. After incubation for 1, 3, 6, or 24 hours, the medium was removed, and cells were washed with D-PBS(−) and detached by trypsinization. The cell suspension was transferred to a 2.0 mL tube and washed three more times with D-PBS(−). Finally, the cells were resuspended in 250 μL of FACS buffer (D-PBS(−) containing 2% FBS). Fluorescent signals were acquired using a flow cytometer (CytoFLEX, Beckman Coulter, Tokyo, Japan) and analyzed using the CytExpert software. For confocal imaging, the HaCaT, A375, and B16 melanoma cells were seeded at 1×10^5 cells mL^{-1} onto glass-bottom dishes (IWAKI, Chiba, Japan) and cultured overnight at 37 °C and 5% CO_2. After replacing the medium with a serum-free medium, DiI-labeled TLNPs-ICG were added at a final concentration of 50 μg mL^{-1}, and the cells were incubated for 1, 3, 6, or 24 hours. Endosome/lysosomal compartments and the nucleus were stained with LysoTracker™ Green DND-26 (excitation wavelength: 504 nm, emission wavelength: 511 nm) and Hoechst 33342 (excitation wavelength: 352 nm, emission wavelength: 461 nm), respectively. After staining, cells were washed twice with FBS-containing medium, overlaid with 1.0 mL of fresh medium, and observed using a fluorescence microscope (FLUOVIEW FV3000, Olympus Corp., Tokyo, Japan). Hoechst 33342, LysoTracker™ Green DND-26, and DiI-labeled TLNPs were excited with lasers at 405, 488, and 561 nm, respectively.

Cytotoxicity evaluation and photothermal effect of TLNPs-ICG

The cytotoxicity of TLNPs was first evaluated *in vitro*. The HaCaT, A375, and B16 melanoma cells were seeded in 96-well plates (3×10^4 cells mL^{-1}, Nippon Genetics Co., Ltd, Tokyo, Japan) and cultured overnight at 37 °C in a humidified 5% CO_2 atmosphere. The culture medium was then replaced with serum-free medium, and the cells were exposed to TLNPs (final protein concentrations: 10, 50, 100, and 200 μg mL^{-1}) or free ICG solution (final concentrations: 10, 20, and 50 μg mL^{-1}). After 24 h of incubation at 37 °C and in 5% CO_2 atmosphere, 10 μL of WST-8 solution (Cell Counting Kit-8, Dojindo Laboratories, Kumamoto, Japan) was added to each well, and the cells were incubated for an additional 2 hours under the same conditions. The absorbance at 450 nm was recorded using a microplate reader (Synergy H1, Agilent BioTek, Tokyo, Japan). Cell viability was calculated by normalizing the absorbance of the treated wells to that of untreated control cells.

Moreover, the photothermal cytotoxicity of TLNPs-ICG in combination with NIR irradiation was evaluated. The A375 and B16 melanoma cells were seeded at 3×10^4 cells mL^{-1} in 96-well plates and cultured overnight at 37 °C and in 5% CO_2 atmosphere. After replacing the medium with a serum-free medium, TLNPs or TLNPs-ICG were added to final concentrations of 10, 50, or 100 μg mL^{-1} and incubated for 22 h under standard culture conditions. Each well was then irradiated with NIR light for 10 min. Immediately after irradiation, 10 μL of WST-8 solution was added to each well and incubated for an additional 2 hours at 37 °C and in 5% CO_2 atmosphere. Absorbance at 450 nm was measured using a microplate reader, and cell viability was expressed as a percentage of the absorbance of treated cells relative to that of untreated controls.

HSP 70 and 90 expression analysis

The A375 and B16 melanoma cells were seeded at 1×10^5 cells mL^{-1} in 24-well plates and incubated overnight at 37 °C in a humidified atmosphere containing 5% CO_2. The medium was then replaced with a serum-free medium, and TLNPs or TLNPs-ICG were added to a final protein concentration of 10 or 50 μg mL^{-1}. After 22 hours of incubation at 37 °C and in 5% CO_2 atmosphere, the cells were exposed to mild hyperthermia at 42 °C and in 5% CO_2 atmosphere for 1 hour, followed by an additional 1 hour of incubation at 37 °C and in 5% CO_2 atmosphere. Cells were harvested by trypsinization and washed three times with PBS to obtain a cell pellet. Total RNA was isolated from the cell pellet using a spin column kit (RNA Basic kit, Nippon Genetics Co., Ltd, Tokyo), and the RNA concentration was measured using a NanoDrop 1000 spectrophotometer (Thermo Fisher Scientific, Tokyo). cDNA was synthesized using PrimeScript™ RT Master Mix (Takara Bio Inc., Shiga, Japan) in a TurboCycler Lite thermal cycler (Blue-Ray Biotech Inc., New Taipei City, Taiwan). Quantitative real-time PCR was then performed using TB Green® Premix Ex Taq™ II with a Thermal Cycler Dice® Real Time System Lite (Takara Bio Inc.) to evaluate the mRNA expression levels of HSP70 and HSP90. The sequences of the various primers used are summarized in SI Table S1.

Antitumor evaluation using tumor-bearing mice

All animal experiments were conducted in accordance with protocols reviewed and approved by the Animal Care and Use Committee of Josai University (approval no. JU24004). In line with the ARRIVE guidelines, efforts were made throughout the study to minimize animal use and discomfort and to ensure ethical handling of all animals. Tumor induction was performed following a described protocol.[31]

C57BL/6 mice were obtained from Sankyo Labo Service Corporation (Tokyo, Japan) and housed in a temperature-controlled room (25 ± 2 °C) under a 12 h light/dark cycle (lights on 9:00–21:00). Animals had free access to MF chow (Oriental Yeast Co., Ltd, Tokyo, Japan) and water. B16 melanoma cells were suspended in PBS, mixed with Geltrex™ (Thermo Fisher Scientific, MA, USA), and adjusted to a final density of 3.3×10^6 cells mL^{-1}. Under anesthesia induced with a mixed anesthetic (medetomidine hydrochloride, 0.15 mg kg^{-1}; butorphanol tartrate, 2.5 mg kg^{-1}), 50 μL of the cell suspension was injected subcutaneously into the flank of each mouse. On day 7 after inoculation, when the tumor volume reached approximately 100 mm^3, TLNPs or TLNPs–ICG were administered intratumorally using a syringe (100 μL per tumor, corresponding to a total protein concentration of 50 μg mL^{-1}). Twenty-two hours after injection, tumors were irradiated with NIR light for 10 min to evaluate the *in vivo* photothermal effect. Skin surface temperature over the tumor was monitored during irradiation using an infrared thermal camera. This injection/irradiation cycle was repeated every 3 days, and antitumor efficacy was assessed over a 14 day period. On day 14, the mice were euthanized, the tumors were excised and weighed, and tissue sections were prepared for the immunohistochemical staining of HSP70 and HSP90 using anti-HSP70 and anti-HSP90.

Statistical analysis

Data are expressed as the mean and standard deviation within the indicated experiment or sample.

Results and discussion

Preparation of tea leaf-derived nanoparticles loaded with indocyanine green (TLNPs-ICG)

TLNPs were isolated from tea leaves by fractionation using a sucrose cushion, as previously reported. The recovered TLNPs had a protein concentration of 2.7 mg mL^{-1} and contained 2.62 μg of EGCG per 100 μg of protein. Dynamic light scattering analysis revealed an average hydrodynamic particle size of approximately 140 nm and a zeta potential of approximately −7.0 mV (Fig. 2a and Table 1). The lipid composition was further analyzed by LC-MS/MS (Fig. S1), showing the relative peak area ratios of each phospholipid fatty acyl species normalized to an internal standard. The phospholipids identified in TLNPs included lysophosphatidylcholine, phosphatidylcholine, lysophosphatidylethanolamine, phosphatidylethanolamine, lysophosphatidylglycerol, phosphatidylglycerol, phosphatidylinositol, phosphatidylserine, and sphingomyelin. These compositions are similar to those reported for other plant-derived nanoparticles, indicating that TLNPs are nanoscale aggregates primarily composed of phospholipids.[28,29]

Next, we prepared ICG-loaded TLNPs (TLNPs-ICG) and characterized their physicochemical properties (Fig. 2a, b and Table 1). After ICG encapsulation, the average particle size increased to approximately 160 nm, and the ζ potential decreased to −11.0 mV. This was attributed to the anionic sulfonic acid groups of ICG. UV-visible spectroscopy revealed a clear absorption maximum around 800 nm only in TLNPs-ICG, confirming the successful encapsulation of ICG into the TLNPs. The amount of ICG encapsulated was 54.4 μg/100 μg of protein, corresponding to an encapsulation efficiency of approximately 54%, indicating the formation of TLNPs-ICG.

Evaluation of the NIR-responsive photothermal effect of TLNPs-ICG

The photothermal heating profile of TLNPs-ICG under 800 nm NIR irradiation is shown in Fig. 3. In dispersions containing

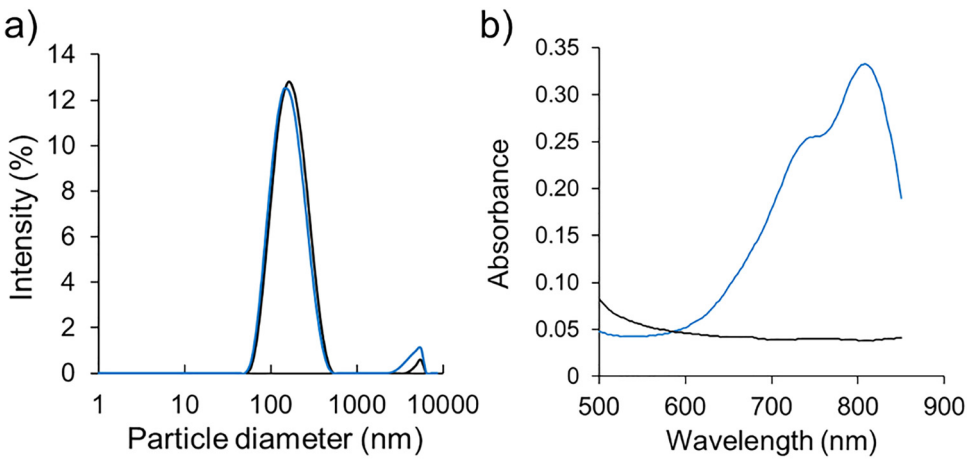

Fig. 2 Characterization of TLNPs and TLNPs-ICG. (a) Diameter of TLNPs and TLNPs-ICG. (b) Absorption spectra of the TLNPs (black line) and TLNPs-ICG (blue line) in PBS. Excitation was performed at 785 nm.

Table 1 Characterization of TLNPs and TLNPs-ICG

Sample	Diameter[a] (nm)	Zeta potential[a] (mV)	ICG amounts[b] (μg/100 μg-protein)	ICG loading rate[b] (%)
TLNPs	142.5 ± 2.4	−6.95 ± 1.0	—	—
TLNPs-ICG	158.4 ± 5.0	−11.0 ± 1.8	54.4 ± 2.17	54.4 ± 2.17

[a] Determined by DLS. [b] Determined by UV-vis. spectroscopy.

TLNPs alone, no appreciable temperature increase was observed upon NIR exposure. By contrast, TLNPs–ICG dispersions exhibited a clear, concentration-dependent photothermal response, in which both the maximum temperature reached increased with the increase in the TLNPs–ICG concentration (Fig. 3a and b). The relationship between the TLNPs–ICG concentration and the peak temperature attained is summarized in Fig. 3c. The data indicated an approximately linear increase in the maximum temperature as a function of the TLNPs–ICG concentration, suggesting that the photothermal effect was governed by the concentration of encapsulated ICG. Notably, at protein-equivalent concentrations of ≥ 50 μg mL^{-1}, TLNPs-ICG achieved temperatures above 43 °C, which is generally considered sufficient for effective photothermal therapy. In addition, the NIR irradiation intensity was varied to 0.5 and 2.0 to confirm the heating effect (Fig. S2). The maximum temperature increased from approximately 35 °C at 0.5 W cm^{-2} to ~54 °C at 2.0 W cm^{-2}. These results demonstrated a clear power-density-dependent heating profile, enabling tunable temperature control to reach the therapeutic window required for PTT. Furthermore, the photothermal conversion efficiency (η) of TLNPs-ICG calculated from the cooling curve was 35.0% (Fig. S2a and b), which was comparable to the reported value[32,33] for ICG-based photothermal agents, supporting the idea that TLNPs-ICG are materials that can be used for photothermal therapy. To assess the stability and reproducibility of the photothermal response, the TLNPs-ICG dispersion was subjected to five consecutive cycles of NIR irradiation (8 min), followed by cooling (12 min). As shown in Fig. 3d, a rapid temperature increase was observed exclusively during NIR irradiation, and the terminal temperature after each 8 min irradiation remained above 43 °C across all five cycles. A slight decrease in the maximum temperature (~2 °C) was observed in the fifth cycle, which was likely attributable to the partial photodegradation of ICG upon repeated irradiation. Importantly, TLNPs-ICG consistently reached temperatures within the effective range for photothermal therapy in every cycle. These findings indicated that TLNPs-ICG could repeatedly generate heat in response to NIR light without the apparent

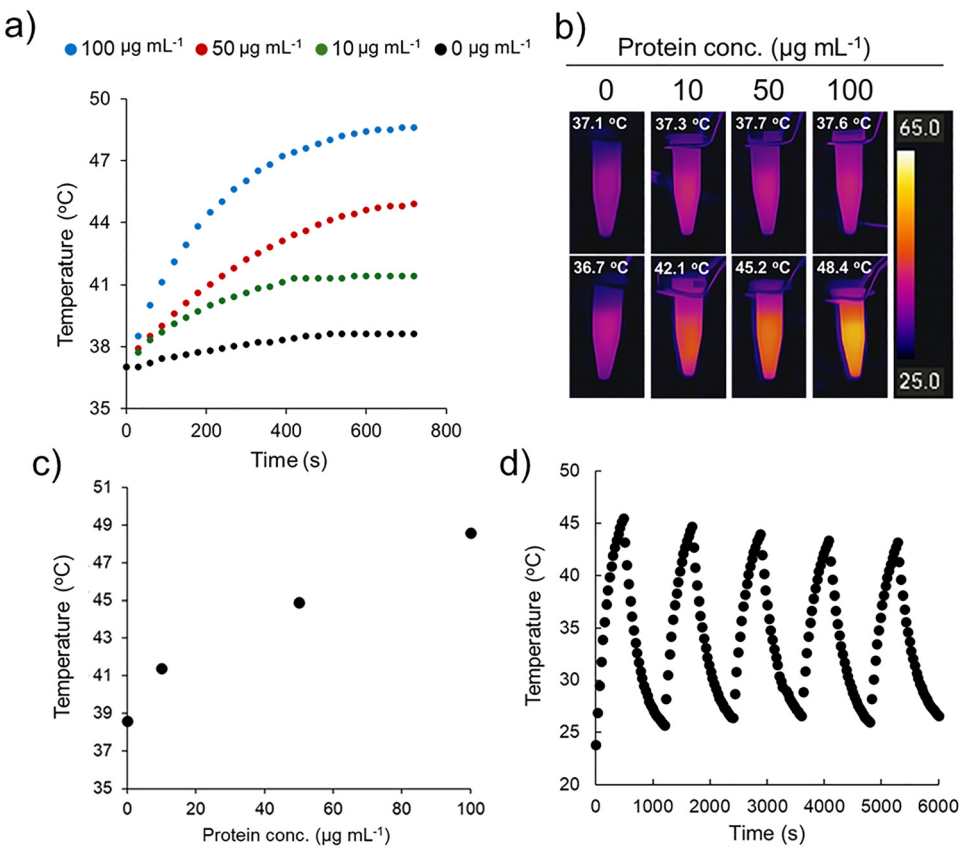

Fig. 3 Characterization of the photothermal effects of TLNPs-ICG. (a) Photothermal effect at each TLNPs-ICG concentration (wavelength of 800 nm and 12 minutes of irradiation). (b) Thermography images of TLNPs-ICG at various concentrations (top: before near-infrared irradiation and bottom: after 12 minutes of near-infrared irradiation). (c) Dependence of the maximum photothermally induced temperature on the TLNPs-ICG concentration. (d) Photothermal effect of TLNPs-ICG by repeated NIR irradiation.

loss of photothermal performance. Collectively, these results demonstrated the successful preparation of TLNPs-ICG as NIR-responsive photothermal nanoparticles suitable for repeated photothermal treatment.

Evaluation of the cellular uptake and cytotoxicity of TLNPs-ICG

The cellular uptake of TLNPs-ICG and its associated effects on cell viability were investigated in normal keratinocytes (HaCaT) and tumor cell lines (A375 and B16 melanoma). Uptake was first assessed by flow cytometry (Fig. 4a). In all three cell types, the fluorescence histogram of the DiO-positive cell population gradually shifted to a high intensity with the increase in the incubation time, indicating the time-dependent cellular uptake of TLNPs-ICG. Consistent with these data, confocal laser scanning microscopy performed 24 hours after exposure to TLNPs-ICG revealed significant intracellular accumulation (Fig. 4b). In merged images, nuclei were stained blue, endosomal/lysosomal compartments were stained green, and TLNPs-ICG were counterstained red. In each cell type, an extensive overlap of green and red fluorescence was observed, indicating that internalized TLNPs-ICG were primarily localized in the endosomal/lysosomal system. These findings suggested that TLNPs-ICG were efficiently internalized by both normal and malignant cells and transported *via* the endocytic vesicle pathway. Because EGCG interacts with the 67 kDa laminin receptor (67LR) and has been suggested to undergo receptor-mediated internalization, the potential contribution of the EGCG/67LR interaction to the TLNPs-ICG uptake was examined by a competition assay (Fig. 4c). The HaCaT cells were seeded and preincubated with various concentrations of EGCG before the addition of TLNPs-ICG. Without the EGCG pretreatment, red fluorescence from TLNPs-ICG was readily detected in punctate structures colocalizing with endosomal/lysosomal markers, consistent with efficient uptake. In contrast, preexposure to EGCG at concentrations of 100 μmol L^{-1} or higher significantly

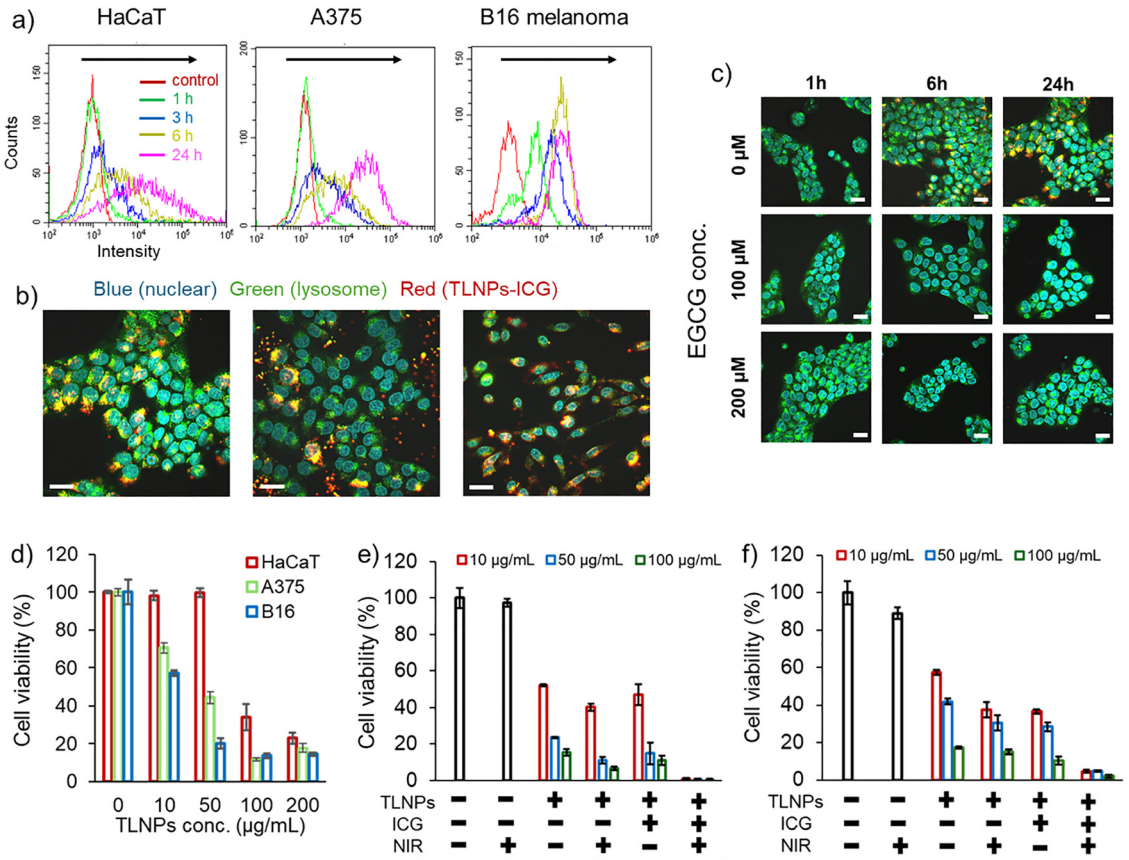

Fig. 4 Evaluation of the cellular uptake and cytotoxicity of TLNPs-ICG. (a) Representative histogram showing results obtained using FACS. The HaCaT, A375 and B16 melanoma cells were treated with 3,3′-dioctadecyloxacarbocyanine perchlorate (DiO)-labeled TLNPs-ICG for 1 (green line), 3 (blue line), 6 (yellow line) and 24 h (pink line). (b) CLSM images of the HaCaT, A375 and B16 melanoma cells treated with 1,1′-dioctadecyl-3,3,3′,3′-tetramethylindocarbocyanine perchlorate (DiI)-labeled TLNPs-ICG (red) for 24 h. Nuclei and lysosomes are stained with Hoechst 33342 (blue) and LysoTracker DND-26 (green), respectively. All scale bars are 20 μm. (c) CLSM images of the HaCaT cells treated with EGCG, followed by 1,1′-dioctadecyl-3,3,3′,3′-tetramethylindocarbocyanine perchlorate (DiI)-labeled TLNPs-ICG (red) for the indicated times. Nuclei and lysosomes were stained with Hoechst 33342 (blue) and LysoTracker DND-26 (green), respectively. All scale bars are 20 μm. (d) Evaluation of the cell viability of the HaCaT, A375, and B16 melanoma cells treated with TLNPs-ICG at various concentrations. Data are expressed as the mean ± SD (n = 3). (e) Evaluation of cell viability by the photothermal effect of TLNPs-ICG on the A375 cells. Data are expressed as the mean ± SD (n = 3). (f) Evaluation of the cell viability by the photothermal effect of TLNPs-ICG on the B16 melanoma cells. Data are expressed as the mean ± SD (n = 3).

reduced or eliminated the intracellular red signal, significantly inhibiting TLNPs-ICG cellular uptake. These observations are consistent with the idea that EGCG saturates or inhibits cell surface 67LR, inhibiting the recognition of the EGCG molecules displayed on TLNPs-ICG. Based on this competitive inhibition, it is suggested that TLNPs-ICG uptake may occur, at least in part, *via* the 67LR-dependent endocytic pathway.

The effects of TLNPs-ICG on cell viability were evaluated in the HaCaT, A375, and B16 melanoma cells (Fig. 4d). The HaCaT cells showed no significant reduction in viability up to 50 μg mL^{-1} (protein equivalent) of TLNPs-ICG, indicating minimal cytotoxicity to normal keratinocytes within this dose range. In contrast, the A375 and B16 melanoma cells showed remarkable sensitivity, with the cell viability of both tumor lines decreasing to less than 50% at 50 μg mL^{-1}. These results revealed a concentration range in which TLNPs-ICG preferentially reduced tumor cell viability while largely avoiding effects on normal cells. This pattern of tumor-selective cytotoxicity is consistent with reports of EGCG-induced antiproliferative effects in malignant cells, suggesting that the inherent cytotoxicity of TLNPs-ICG is primarily due to its EGCG content.

The cytotoxicity of the combined effects of TLNPs-ICG and with/without NIR-induced photothermal heating was evaluated (Fig. 4e and f). NIR irradiation in the absence of TLNPs-ICG did not affect viability in any of the cell lines tested, confirming that the applied parameters did not damage cells without ICG. In addition, the treatment of cancer cells with free EGCG at a concentration equivalent to the EGCG content in TLNPs-ICG resulted in higher cell viability than that for the treatment with TLNPs-ICG (Fig. S4). This finding suggests that the retention of EGCG within TLNPs may enhance its stability, thereby increasing its effective bioactivity under the experimental conditions. Furthermore, in the absence of NIR, TLNPs-ICG and TLNPs exhibited similar viability profiles, indicating that ICG does not exert significant cytotoxicity under the conditions used. When TLNPs-ICG-treated tumor cells were exposed to NIR irradiation, cell viability dramatically decreased to only a few percent. This significant decrease in viability was consistent with heat-induced cell death caused by the strong photothermal response of TLNPs-ICG. Overall, these results demonstrated that TLNPs-ICG combined EGCG-mediated biochemical cytotoxicity with NIR-responsive photothermal activity and could exert potent antitumor effects *in vitro* when combined with NIR irradiation.

HSP 70 and 90 expression analysis

It is well known that tumor cells acquire thermotolerance through repeated PTT cycles, and the suppression of this thermotolerance is thought to be important for maximizing the effects of PTT. The heat shock proteins, HSP70 and HSP90, are important mediators of thermotolerance, and EGCG has been reported to inhibit their expression. Based on this, we evaluated the changes in the HSP expression at the mRNA level in the A375 and B16 melanoma cells after the TLNPs-ICG treatment (Fig. 5a and b).

When the A375 and B16 melanoma cells were exposed to TLNPs-ICG alone (37 °C, without heat stress), the mRNA

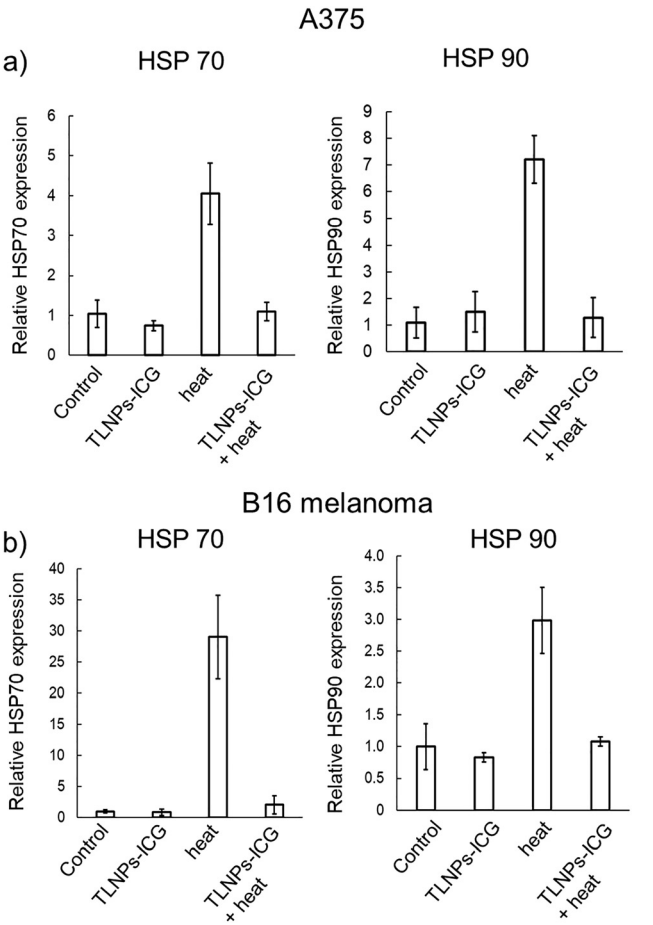

Fig. 5 Evaluation of TLNPs-ICG for suppressing the HSP70 and HSP90 expressions at the mRNA level. (a) Expression analysis of HSP70 (left) and HSP90 (right) in the A375 cells. Data are expressed as the mean ± SD (n = 3). (b) Expression analysis of HSP70 (left) and HSP90 (right) in the B16 melanoma cells. Data are expressed as the mean ± SD (n = 3).

expression levels of HSP70 and HSP90 were comparable to those of the untreated control, indicating that TLNPs-ICG did not alter the basal expression of HSPs. In contrast, when cells were hyperthermia-treated at 42 °C, a clear upregulation of HSP70 and HSP90 was observed in the A375 and B16 melanoma cells, confirming the activation of a typical heat shock response to heat stress. On the other hand, when heat treatment was performed in the presence of TLNPs-ICG, the heat-induced increase in the HSP70 and HSP90 expression was significantly attenuated, with expression levels comparable to those in the non-heated control group. This suppression of HSP induction in the TLNPs-ICG/heat-treated group was consistent with the known ability of EGCG to downregulate HSP70 and HSP90, suggesting that EGCG delivered *via* TLNPs-ICG inhibited the cellular heat shock response.

Integrated findings from these *in vitro* evaluations suggested that TLNPs–ICG functioned not only as a photothermal agent but also as an EGCG carrier, thereby suppressing the heat-stress–induced upregulation of the HSP expression at the mRNA level. This dual action inhibited the development of thermotolerance during repeated PTT cycles, potentially

contributing to the realization of more effective and sustained antitumor photothermal therapy.

Antitumor evaluation using tumor-bearing mice

In vivo antitumor activity was evaluated using a B16 melanoma tumor-bearing mouse model (Fig. 6). Treatment began when the tumor volume reached approximately 100 mm^3. Each formulation was administered *via* intratumoral injection (100 μL per tumor) using a syringe. During subsequent NIR light irradiation, the temperature near the tumor was monitored (Fig. 6a). In mice administered ICG-free TLNPs, no significant increase in tumor temperature was observed upon NIR exposure, indicating the absence of carrier-specific photothermal activity. In contrast, in mice administered free ICG or TLNPs-ICG, a clear NIR-responsive heating profile was detected, with tumor temperature increasing to approximately 43 °C. This temperature range was considered suitable for photothermal therapy (PTT), suggesting that PTT-related hyperthermia can be achieved under the applied conditions. No significant weight change or obvious systemic toxicity was observed in any group throughout the experimental period (Fig. 6b). The anti-tumor effects are summarized in Fig. 6c and d. Based on the longitudinal analysis of tumor volume (Fig. 6c), tumors in the free ICG group grew at a rate similar to that of the D-PBS control group, indicating that ICG alone could not suppress tumor progression under these conditions. In the TLNP, TLNPs-ICG, and TLNP + NIR groups, tumor growth was delayed compared with that in the control group, but maintained an overall increasing trend. This trend was consistent with the reported anticancer effects of EGCG and tea leaf-derived nanoparticles, suggesting moderate growth-suppressing activity. A similar tumor growth-suppressing effect was observed in the ICG + NIR group, likely due to photothermal damage. However, because NIR irradiation in this experiment was performed every 3 days under relatively mild conditions, the tumors showed net growth over time. Surprisingly, a significant decrease in tumor volume was observed only in the TLNPs-ICG + NIR group, with a reduction of approximately 50% compared to the initial tumor volume. This remarkable tumor growth inhibition was likely due to the synergistic interaction between EGCG-mediated biochemical effects and ICG-induced photothermal heating, enabling effective tumor suppression even under an intermittent (3 day cycle) treatment schedule. Similarly, the analysis of mean tumor weight on day 12 revealed that only the TLNPs-ICG + NIR group exhibited a significantly lower tumor mass compared to the other groups (Fig. 6d). In addition, the survival curves for each treatment group showed a progressive decrease in survival, which was associated with tumor growth, whereas only the TLNPs-ICG + NIR group maintained 100% survival over the extended observation period, indicating a pronounced therapeutic benefit (Fig. S5). Moreover, in conjunction with the longitudinal body-weight profiles (Fig. 6b), the concomitant reduction in tumor volume and improvement in survival suggest that the treatment did not elicit overt systemic toxicity or severe adverse effects under the tested conditions.

To further explore the underlying mechanisms associated with thermotolerance, tumor sections excised at the end of the

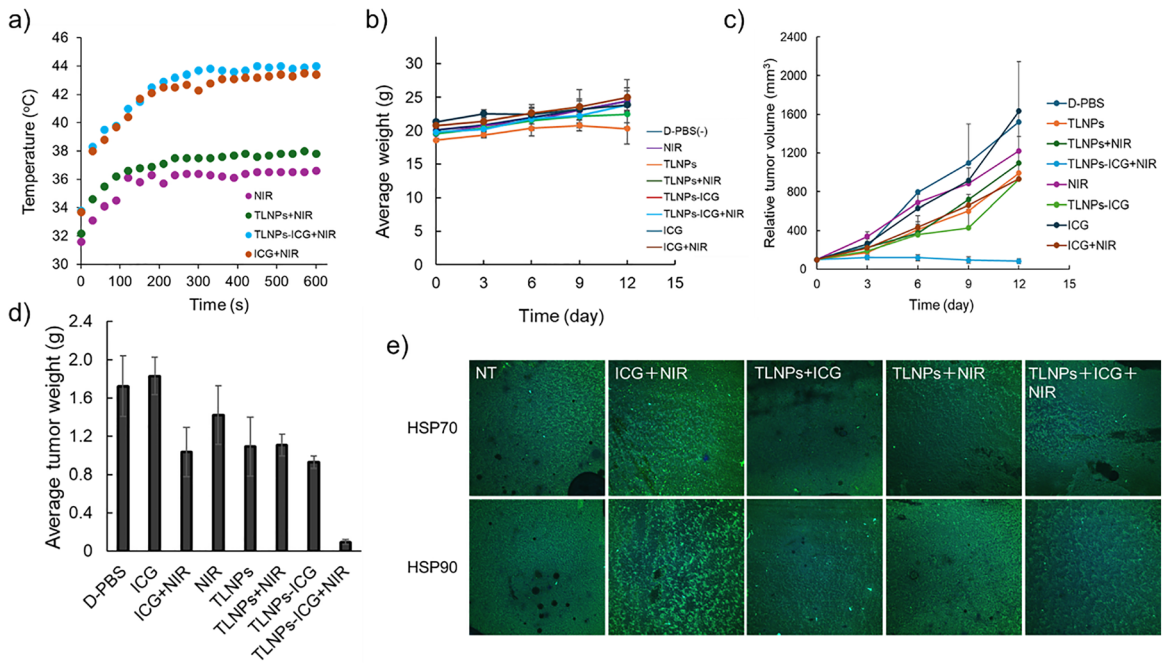

Fig. 6 *In vivo* antitumor evaluation. (a) Tumor surface temperature during NIR light irradiation. (b) Time-course of mean body weight in mice for each treatment group. Data are expressed as the mean ± SD (n = 3). (c) Tumor growth in B16 melanoma–bearing mice. B16 melanoma cells were inoculated subcutaneously into the dorsal region of C57BL/6 mice, and treatment was initiated when the tumor volume reached approximately 100 mm^3. Data are presented as the mean ± SD (n = 4). (d) Tumor volume for each treatment group on day 12 after treatment initiation. Data are presented as the mean ± SD (n = 4). (e) Merged confocal laser scanning microscopy images of fluorescent immunostaining for HSP70 and HSP90 in tumor sections excised at the end of the treatment period. Blue: DAPI and green: HSP70 or HSP90.

study were subjected to immunofluorescence staining for HSP70 and HSP90 and analyzed by CLSM (Fig. 6e). In the ICG + NIR group, both HSP70- and HSP90-derived green fluorescence signals were significantly enhanced, indicating the induction of heat shock proteins in response to photothermal stress. In contrast, in the TLNPs-ICG + NIR group, no obvious enhancement of HSP70- or HSP90-derived fluorescence was detected, despite tumor heating during NIR irradiation, and the staining pattern was comparable to that observed in the untreated (NT) control group. These findings suggested that the presence of TLNPs-ICG in the tumor microenvironment suppressed heat-induced HSP expression *in vivo*, which was consistent with *in vitro* observations. Collectively, these results suggested that TLNPs-ICG exhibited efficient photothermal activity while concurrently suppressing HSP70/90 expression, thereby attenuating the acquisition of thermotolerance. Although tumor-volume reduction by PTT has also been reported,[27] the present model enables comparable antitumor outcomes with a relatively short NIR irradiation duration and few administrations of TLNPs-ICG. This improvement was likely attributable to the combined contributions of maintaining temperatures within the therapeutically effective photothermal window, the intrinsic antitumor activity of TLNPs, and the suppression of the HSP expression, which mitigated thermotolerance. In synergy with their tumor-selective cytotoxic activity, these complementary functions are expected to enhance the overall antitumor efficacy of PTT in this model.

Conclusion

In this study, we developed tea leaf-derived nanoparticles (TLNPs) that efficiently encapsulated near-infrared dye indocyanine green (ICG), thereby synthesizing TLNPs-ICG, which exhibited stable, concentration-dependent photothermal activity under 800 nm irradiation. TLNPs-ICG were readily internalized by both normal keratinocytes and melanoma cells, at least in part, *via* the EGCG-67 kDa laminin receptor. At moderate concentrations, they exhibited dose-dependent cytotoxicity, preferentially reducing tumor cell viability while sparing normal cells. When combined with near-infrared irradiation, TLNPs-ICG induced potent photothermal cytotoxicity, whereas TLNPs or ICG alone (with or without NIR irradiation) had limited antitumor effects. Furthermore, TLNPs-ICG suppressed the hyperthermia-induced upregulation of HSP70 and HSP90 in tumor tissues *in vitro* and *in vivo*, suggesting that they effectively inhibited the acquisition of thermotolerance during repeated photothermal therapy. In a B16 melanoma mouse model, the intratumoral administration of TLNPs-ICG, combined with intermittent NIR irradiation, achieved significant tumor growth inhibition without apparent systemic toxicity. These findings suggested that TLNPs-ICG functioned as biologically derived photothermal biomaterials, integrating EGCG-mediated biochemical antitumor activity with ICG-driven photothermal heating and HSP suppression. Therefore, tea leaf-derived nanoparticles hold promise as edible plant-based functional materials for next-generation combined photothermal cancer therapy because they are naturally enriched with EGCG and present a vesicle architecture that supports intrinsic anticancer activity.

Author contributions

The manuscript was written through contributions from all authors who gave their approval to the final version. Keito Suzuki: investigation, formal analysis, data curation, and writing – review & editing. Syuuhei Komatsu: writing – review & editing, writing – original draft, project administration, methodology, investigation, formal analysis, data curation, and conceptualization. Kanae Ishii: investigation, formal analysis, and data curation. Kaho Tanaka: investigation, formal analysis, and data curation. Yuka Kiba: investigation and formal analysis. Masashi Kitamura: formal analysis and writing – review & editing. Toru Kimura: investigation and formal analysis. Ryuichiro Suzuki: investigation, formal analysis, and writing – review & editing. Takashi Tanikawa: formal analysis and writing – review & editing. Kazuya Oki: investigation and formal analysis. Atsushi Takahashi: formal analysis and writing – review & editing. Hiroaki Todo: writing – review & editing, project administration, methodology, and conceptualization.

Conflicts of interest

There are no conflicts to declare.

Data availability

All the data supporting the findings will be made public and can be obtained by contacting the corresponding author, H. Todo.

Supplementary information (SI) is available. Method of phospholipid analysis by LC–MS/MS. Method of calculation of photothermal conversion efficiency. Table S1 Sequences of various primers used for HSP measurement. Fig. S1 Analysis of phospholipids in TLNPs by liquid chromatography-tandem mass spectrometry (LC–MS/MS). Fig. S2 Photothermal effect of TLNPs-ICG at different irradiation intensities. Fig. S3 Calculation of photothermal conversion efficiency. Fig. S4 Cell viability in each cancer cell line after treatment with free EGCG at a dose equivalent to the EGCG content in TLNPs-ICG. Fig. S5 Survival curves of tumor bearing mice treated with D-PBS (−), NIR only, TLNPs, TLNPs + NIR, TLNPs–ICG, TLNPs–ICG + NIR, free ICG, or free ICG + NIR. See DOI: https://doi.org/10.1039/d6tb00055j.

References

1 P. Wust, B. Hildebrandt, G. Sreenivasa, B. Rau, J. Gellermann, H. Riess, R. Felix and P. M. Schlag, Hyperthermia in combined treatment of cancer, *Lancet Oncol.*, 2002, **3**, 487–497, DOI: 10.1016/S1470-2045(02)00818-5.

2 F. Qi, Q. Bao, P. Hu, Y. Guo, Y. Yan, X. Yao and J. Shi, Mild magnetic hyperthermia-activated immuno-responses for primary bladder cancer therapy, *Biomaterials*, 2024, **307**, 122514, DOI: 10.1016/j.biomaterials.2024.122514.

3 H. Luo and S. Gao, Recent advances in fluorescence imaging-guided photothermal therapy and photodynamic therapy for cancer: from near-infrared-I to near-infrared-II, *J. Controlled Release*, 2023, **362**, 425–445, DOI: 10.1016/j.jconrel.2023.08.056.

4 T. Zhang, P. Wei, M. Suo, P. You, R. Huang, J. Chen, M. Lyu, N. Zhang, S. Ning and B. Z. Tang, Stimuli-Responsive Hydrogels Potentiating Photothermal Therapy against Cancer Stem Cell–Induced Breast Cancer Metastasis, *ACS Nano*, 2024, **18**, 20313–20323, DOI: 10.1021/acsnano.4c04067.

5 G. Gao, X. Sun and G. Liang, Nanoagent-Promoted Mild-Temperature Photothermal Therapy for Cancer Treatment, *Adv. Funct. Mater.*, 2021, **31**, 2100738, DOI: 10.1002/adfm.202100738.

6 J. You, R. Zhang, G. Zhang, M. Zhong, Y. Liu, C. S. Van Pelt, D. Liang, W. Wei, A. K. Sood and C. Li, Photothermal-chemotherapy with doxorubicin-loaded hollow gold nanospheres: a platform for near-infrared light-triggered drug release, *J. Controlled Release*, 2012, **158**, 319–328, DOI: 10.1016/j.jconrel.2011.10.028.

7 R. Rosenzweig, N. B. Nillegoda, M. P. Mayer and B. Bukau, The Hsp70 chaperone network, *Nat. Rev. Mol. Cell Biol.*, 2019, **20**, 665–680, DOI: 10.1038/s41580-019-0133-3.

8 M. Zhou, C. Zhou, H. Geng, Z. Huang, Z. Lin, Y. Wang, Y. Zhu, J. Shi, J. Tan, L. Guo, Y. Zhao, Y. Zhang, Q. Peng, H. Yu, W. Dai, H. Lv and Z. Lin, EGCG-enabled Deep Tumor Penetration of Phosphatase and Acidity Dual-responsive Nanotherapeutics for Combinatory Therapy of Breast Cancer, *Small*, 2025, **21**, 2406245, DOI: 10.1002/smll.202570104.

9 P. Wu, H. Zhang, Y. Yin, M. Sun, S. Mao, H. Chen, Y. Deng, S. Chen, S. Li and B. Sun, Engineered EGCG-Containing Biomimetic Nanoassemblies as Effective Delivery Platform for Enhanced Cancer Therapy, *Adv. Sci.*, 2022, **9**, 2105894, DOI: 10.1002/advs.202105894.

10 L. Zeng, J. Yan, L. Luo, M. Ma and H. Zhu, Preparation and characterization of (−)-Epigallocatechin-3-gallate (EGCG)-loaded nanoparticles and their inhibitory effects on human breast cancer MCF-7 cells, *Sci. Rep.*, 2017, **7**, 45521, DOI: 10.1038/srep45521.

11 Y. Fujimura, M. Sumida, K. Sugihara, S. Tsukamoto, K. Yamada and H. Tachibana, Green Tea Polyphenol EGCG Sensing Motif on the 67 kDa Laminin Receptor, *PLoS One*, 2012, **7**, e37942, DOI: 10.1371/journal.pone.0037942.

12 H. Tachibana, Green Tea Polyphenol Epigallocatechin-3-gallate Signaling Pathway through 67 kDa Laminin Receptor, *Folia Pharmacol. Jpn.*, 2008, **132**, 145–149, DOI: 10.1254/fpj.132.145.

13 P. L. C. H. B. Tran, S.-A. Kim, H. S. Choi, J.-H. Yoon and S.-G. Ahn, Epigallocatechin-3-gallate suppresses the expression of HSP70 and HSP90 and exhibits anti-tumor activity in vitro and in vivo, *BMC Cancer*, 2010, **10**, 276, DOI: 10.1186/1471-2407-10-276.

14 Z. Yin, E. C. Henry and T. A. Gasiewicz, (−)-Epigallocatechin-3-gallate is a novel Hsp90 inhibitor, *Biochemistry*, 2009, **48**, 336–345, DOI: 10.1021/bi801637q.

15 Z.-Y. Chen, Q.-Y. Zhu, Y. F. Wong, Z. Zhang, H. Y. Chung and H. Chung, Stabilizing effect of ascorbic acid on green tea catechins, *J. Agric. Food Chem.*, 1998, **46**, 2512–2516, DOI: 10.1021/jf971022g.

16 Q. Wang, J. Cao, H. Yu, J. Zhang, Y. Yuan, W. Liao and C. Li, The effects of EGCG on the mechanical, bioactivities, cross-linking and release properties of gelatin film, *Food Chem.*, 2019, **271**, 204–210, DOI: 10.1016/j.foodchem.2018.07.168.

17 Z. Wei, W. Yang, R. Fan, F. Yuan and Y. Gao, Evaluation of structural and functional properties of protein–EGCG complexes and their ability of stabilizing a model β-carotene emulsion, *Food Hydrocolloids*, 2015, **45**, 337–350, DOI: 10.1016/j.foodhyd.2014.12.008.

18 W. Liu, A. Ye, F. Han and J. Han, Advances and challenges in liposome digestion: surface interaction, biological fate, and GIT modeling, *Adv. Colloid Interface Sci.*, 2019, **263**, 52–67, DOI: 10.1016/j.cis.2018.11.007.

19 W. Dai, C. Ruan, Y. Zhang, J. Wang, J. Han, Z. Shao, Y. Sun and J. Liang, Bioavailability enhancement of EGCG by structural modification and nano-delivery: a review, *J. Funct. Foods*, 2020, **65**, 103732, DOI: 10.1016/j.jff.2019.103732.

20 J. Feng, Q. Xiu, Y. Huang, Z. Troyer, B. Li and L. Zheng, Plant-Derived Vesicle-Like Nanoparticles as Promising Biotherapeutic Tools: Present and Future, *Adv. Mater.*, 2023, **35**, e2207826, DOI: 10.1002/adma.202207826.

21 B. Zhao, H. Lin, X. Jiang, W. Li, Y. Gao, M. Li, Y. Yu, N. Chen and J. Gao, Exosome-like nanoparticles derived from fruits, vegetables, and herbs: innovative strategies of therapeutic and drug delivery, *Theranostics*, 2024, **14**, 4598–4621, DOI: 10.7150/thno.97096.

22 H. A. Dad, T. W. Gu, A. Q. Zhu, L. Q. Huang and L. H. Peng, Plant Exosome-like Nanovesicles: Emerging Therapeutics and Drug Delivery Nanoplatforms, *Mol. Ther.*, 2021, **29**, 13–31, DOI: 10.1016/j.ymthe.2020.11.030.

23 E.-G. Cho, S.-Y. Choi, H. Kim, E.-J. Choi, E.-J. Lee, P.-J. Park, J. Ko, K. P. Kim and H. S. Baek, Panax ginseng-Derived Extracellular Vesicles Facilitate Anti-Senescence Effects in Human Skin Cells: An Eco-Friendly and Sustainable Way to Use Ginseng Substances, *Cells*, 2021, **10**, 486, DOI: 10.3390/cells10030486.

24 F. Bahri, M. Mansoori, S. Vafaei, S. Fooladi, Y. Mir, M. Mehrabani, Y. Hozhabri, M. H. Nematollahi and S. Iravani, A comprehensive review on ginger-derived exosome-like nanoparticles as feasible therapeutic nano-agents against diseases, *Mater. Adv.*, 2024, **5**, 1846–1867, DOI: 10.1039/D3MA00856H.

25 K. Moon, J. Hur, K. P. Kim, K. Lee and J. Y. Kang, Surface-Functionalizable Plant-Derived Extracellular Vesicles for Targeted Drug Delivery Carrier Using Grapefruit, *Adv. Mater. Interfaces*, 2023, **10**, e2300220, DOI: 10.1002/admi.202300220.

26 S. Ju, J. Mu, T. Dokland, X. Zhuang, Q. Wang, H. Jiang, X. Xiang, Z.-B. Deng, B. Wang, L. Zhang, M. Roth, R. Welti,

J. Mobley, Y. Jun, D. Miller and H.-G. Zhang, Grape exosome-like nanoparticles induce intestinal stem cells and protect mice from DSS-induced colitis, *Mol. Ther.*, 2013, **21**, 1345–1357, DOI: 10.1038/mt.2013.64.

27 L. Zeng, H. Wang, W. Shi, L. Chen, T. Chen, G. Chen, W. Wang, J. Lan, Z. Huang, J. Zhang and J. Chen, Aloe derived nanovesicle as a functional carrier for indocyanine green encapsulation and phototherapy, *J. Nanobiotechnol.*, 2021, **19**, 439, DOI: 10.1186/s12951-021-01195-7.

28 Q. Chen, M. Zu, H. Gong, Y. Ma, J. Sun, S. Ran, X. Shi, J. Zhang and B. Xiao, Tea leaf-derived exosome-like nanotherapeutics retard breast tumor growth by pro-apoptosis and microbiota modulation, *J. Nanobiotechnol.*, 2023, **21**, 6, DOI: 10.1186/s12951-022-01755-5.

29 D. Sasaki, K. Kusamori, Y. Takayama, S. Itakura, H. Todo and M. Nishikawa, Development of nanoparticles derived from corn as mass producible bionanoparticles with anticancer activity, *Sci. Rep.*, 2021, **11**, 22818, DOI: 10.1038/s41598-021-02241-y.

30 M. Hashimoto, S. Itakura, K. Kusamori, K. Yajima, S. Mitsuhashi, S. Hayashi, H. Todo and M. Nishikawa, Therapeutic Potential of Rose Hip-Derived Nanoparticles for Psoriatic Skin Inflammation, *ACS Biomater. Sci. Eng.*, 2025, **11**, 5938–5951, DOI: 10.1021/acsbiomaterials.5c00826.

31 A. Ito, S. Itakura, Y. Hasegawa, M. Hashimoto, A. Okada, M. Hirafuji, H. Nakamura, K. Sugibayashi and H. Todo, Usefulness of direct intratumoral administration of doxorubicin hydrochloride with an electro-osmosis–assisted pump, *Front. Drug Delivery*, 2023, **3**, 1150894, DOI: 10.3389/fddev.2023.1150894.

32 Z. Liu, X. Deng, Z. Wang, Y. Guo, M. M. A. Hameed, M. EL-Newehy, J. Zhang, X. Shi and M. Shen, A biomimetic therapeutic nanovaccine based on dendrimer–drug conjugates coated with metal–phenolic networks for combination therapy of nasopharyngeal carcinoma: an in vitro investigation, *J. Mater. Chem. B*, 2025, **13**, 5440–5452, DOI: 10.1039/D5TB00226E.

33 Z. Li, J. Lan, L. Liu, Y. Wang, L. Chen, R. Zeng, D. Gu, R. Hu, T. Zhang and Y. Ding, Versatile Thermo-Sensitive liposomes with HSP inhibition and Anti-Inflammation for synergistic Chemo-Photothermal to inhibit breast cancer metastasis, *Int. J. Pharm.*, 2024, **664**, 124583, DOI: 10.1016/j.ijpharm.2024.124583.